A FORMULATION FOR UNSUPERVISED HIERARCHICAL SEGMENTATION OF FACADE IMAGES WITH PERIODIC MODELS

Jean-Pascal Burochin, Bruno Vallet, Olivier Tournaire and Nicolas Paparoditis

Université Paris-Est, Institut Géographique National, Laboratoire *MATIS*
73 Avenue de Paris, 94165 Saint-Mandé Cedex, France, {firstname.lastname}@ign.fr

Commission III/4

KEY WORDS: street level imagery, facade reconstruction, unsupervised hierarchical segmentation, gradient accumulation, recursive split, model matching, periodicity detection

ABSTRACT:

We introduce an unsupervised segmentation method to build a hierarchical representation of a building facade from a single calibrated street level image. The process recursively splits horizontally or vertically the rectified image along dominant alignments until the radiometric content of the region hypothesis corresponds to a given model. This paper propose two main novelties: first we describe an advanced split energy formulation to separate dominant alignments breaks. Then we introduce a model that express periodicity in facade texture. This segmentation could be an interesting tool for facade modeling and is in particular well suited for facade texture compression.

1 INTRODUCTION

1.1 Context

Facade analysis (detection, understanding and field of reconstruction) from street level imagery is currently a very active field of research in photogrammetric computer vision due to its many applications. Facade models can for instance be used to increase the level of details of 3D city models generated from aerial or satellite imagery. They also are useful for a compact coding of facade image textures for streaming or for an embedded system. The characterization of stable regions in facades is also necessary for robust indexation and image retrieval.

We work exclusively on a single calibrated street-level image. We voluntarily did not introduce additional information such as 3D imagery (point clouds, etc.) because for some applications such as indexation, image retrieval and localization, we could just have a single photo acquired by a mobile phone.

1.2 Previous work

Existing facade extraction frameworks are frequently specialized for a certain type of architectural style or a given texture appearance. In a procedural way, operators often step in a pre-process to split correctly the image into suitable regions. Studied images indeed are assumed to be framed in such a way that they exactly contain relevant information data such as windows on a clean wall background.

Most building facade analysis techniques try to extract specific shapes/objects from the facade: windows frame, etc. Most of them are data driven (Ali et al., 2007, Lee and Nevatia, 2004, Haugeard et al., 2009), *i.e.* image features are first extracted and then some models are matched by them to build object hypotheses. Some other model-driven techniques such as (Korah and Rasmussen, 2007), (Reznik and Mayer, 2007) or (Han and Zhu, 2005) try to find more complex objects which are patterns or layouts of simple objects (*e.g.* alignments in 1D or in 2D). Higher level techniques such as (Alegre and Dellaert, 2004), (Müller et al., 2007) and (Ripperda, 2008) try to generate directly a hierarchy of complex objects composed of patterns of simple objects usually with grammar-based approaches. Those methods generally devote their strategy to a special architectural style.

Finally, (Burochin et al., 2009) propose a facade segmentation independent of its architectural style. This framework first separates a facade from its background and neighboring facades, and then identifies intra-facade regions of specific elementary texture models that all facades have in common. A recursive segmentation is applied only directed by dominant alignments. Neighboring facades and main intern shapes are correctly separated without any semantic *a priori*. But detected models do not concerns repeated structures, that are tipical properties of man-made objects, such as described in (Wenzel et al., 2008).

1.3 Contribution

Most of the aforementioned approaches are specialized in a particular kind of architecture. Few of them have addressed very complex facade networks such as the ones encountered in European cities where the architectural diversity and complexity is large (Hausmannian buildings for instance or other complex architectures with balconies or decoration elements). Our work is upstream from most of these approaches and improves on the recent framework proposed by (Burochin et al., 2009) (our contribution is mentioned in red on figure 1). We summarize this previous approach in section 2. Section 3 explains our new split energy formulation that better separates dominant alignment breaks. Then section 4 introduces a third model: the periodic one. We eventually present some results in section 5 and we discuss them.

2 GENERAL STRATEGY

In this section we describe the general strategy of (Burochin et al., 2009). This strategy requires horizontal and vertical image contour alignments. Thus images first are rectified in the facade plane using two vanishing points extracted as described in (Kalantari et al., 2008). The segmentation relies on a recursive split process and on a model based analysis of each subdivided regions. If the considered region does not match any of the proposed models, it is split into two sub-regions which are later analyzed as illustrated

by the decision tree on figure 1. Models are based on radiometric criteria: planes and generalized cylinders. Such objects are representative of frequent facade elements like repetitive window panes, wall background or cornices. The process is explained in follows.

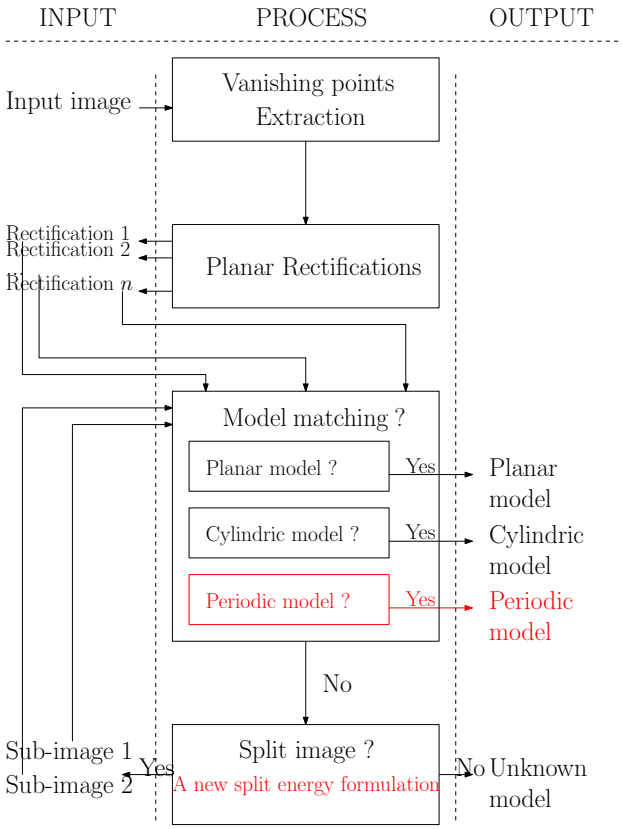

Figure 1: Hierarchical unsupervised segmentation: algorithm recursively confronts data with models. Regions that do not match any proposed model are split. Contribution of this article is mentioned in red.

2.1 Model Matching

The problem is to recognize some proposed models in the facade. Given an image region, intensity is compared to one of these models in increasing complexity order: the planar model, then the generalized cylinders. The process stops when the sub-image is considered as a good match for the model: we simply count local radiometric differences as follows. Let I_k be the sub-image at region R_k of a façade image I. Sub-image I_k is described by model $\mathcal{M}$ when the deviation $N_{\mathcal{M}}(I_k)$ is small enough and if this model is the simplest one. Deviation $N_{\mathcal{M}}(I_k)$ is defined by the number of pixels whose radiometry differs too much from the model.

The planar model assumes that the intensity of the sub-image I_k at pixel p follows an uniform radiometry: $I_k(p) = \lambda + \epsilon(p)$ with λ being the uniform radiometry and $\epsilon(p)$ being noise (small local details, sparse occlusions or Gaussian noise). The generalized cylinders are designed either in columns or in rows. The cylindric model in columns for instance assumes intensities to follow $I_k(x, y) = \lambda(x) + \epsilon(x, y)$ with $\lambda(x)$ being the cylinder value and $\epsilon(x, y)$ being noise. Figure 2 illustrates instances of such models.

2.2 Split Process

Regions that do not match any model are split horizontally or vertically. With a technique close to (Lee and Nevatia, 2004),

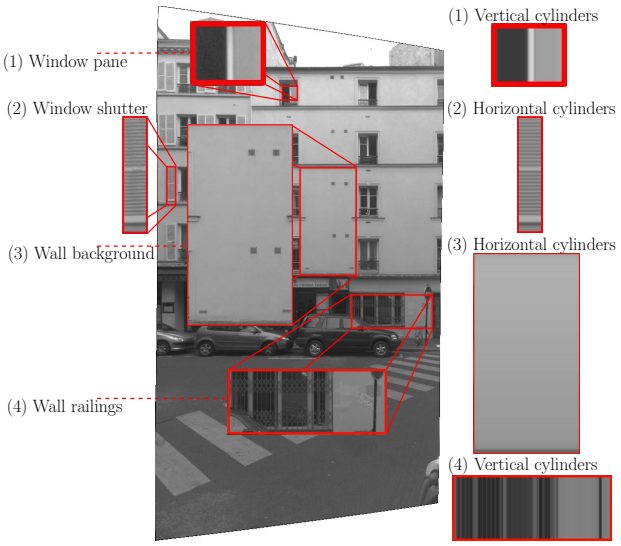

Figure 2: Instances of radiometric cylindric models: vertical cylinders can be detected in window pane or wall railings, horizontal cylinders in window shutter or wall background

horizontal and vertical dominant alignments are respectively detected at maxima of vertical and horizontal profiles of gradient accumulation, vertical profile being obtained by horizontal gradients. This enforces low but repetitive contrasts.

The split strategy relies on structures alignment break between two facades or inside one facade. Split hypotheses are the previous detected dominant alignments. If such a vertical hypothesis is located at x_0, horizontal dominant alignments are separately detected in the left and right regions. Two new grid patterns are thus constituted by vertical dominant alignments and new horizontal ones. An edge of such a grid pattern that covers enough strong gradients is named *regular edges*. Other ones are *fictive edges*: falsely detected edges. The best splitting hypothesis minimizes the length of *fictive edges* in each of the two sub-region. Figure 3a shows such split process optimization.

3 SPLIT ENERGY ADVANCEMENT

The strength of dominant alignment usage is its independence to local isolated structures. (Burochin et al., 2009) aims at minimizing such alignments in best split selection. But alignments of edges at two different scales are then compared. They do not deal with the same structure types. For instance on figure 3a, the fictive edges of the top region nearly coincide with the ones of the whole region whereas bottom region contains long contaminating *fictive edges* generated by local high contrasts that were insignificant in the whole region. Split energy at this hypothesis is negative. Yet it is precisely the split location we are looking for. In this typical case, an information about a road sign is compared to alignment of window borders.

3.1 Optimization in Edges Space

We propose in this paper a static edges structure based split optimization. We have chosen the solution to study edges distribution only with dominant alignments grid pattern of the whole region unlike approach of (Burochin et al., 2009). We build an *edges space* based on this grid pattern. Now let us introduce the *horizontal edges space*.

Let $(x_j)_{j\in[|0,n|]}$ be the vertical dominant alignment set such that $x_n - x_0$ is the region width.

Figure 3: Alignment breaks detection. Vertical distribution profile in red on left side of images is *split energy* intensities in function of the split hypothesis ordinate. Positive values are inside considered region, negative are outside. *Fictive edges* in the whole region are illustrated in yellow. a) Comparison of dominant alignments in both sub-region: *fictive edges* of sub-regions are illustrated in red. b) Optimization in static edges space.

We name $h_{i,j} = \left[\binom{x_{j-1}}{y_i}; \binom{x_j}{y_i}\right]$ the edge located along the dominant alignment y_i and between alignments x_{j-1} and x_j.

Let c_h be the $0, 1$ coloring distribution of the *regular edges* along horizontal edges: $c_h(i,j)$ is 1 if the edge $h_{i,j}$ is a *regular edge* and 0 otherwise.

The *vertical edges space* is identically defined in the other dimension. The best split hypothesis for us is the highest split energy one given by equation 1: the best horizontal or vertical split.

$$max(E_x^*(c), E_y^*(c)) \tag{1}$$

Split energy is described by two energy terms: the *intra-region* energy (E_{intra}) and the *inter-region* energy (E_{inter}). The former measures information located into both sub-regions. The latter measures information along the dominant alignment that separates them. Split energy is computed in the *edges space*. Equation 2 defines the best vertical split hypothesis. A similar computing is used to detect the best horizontal split hypothesis.

$$E_x^*(c) = \max_k(\alpha f(E_{intra}(x_k, c)) + (1-\alpha) g(E_{inter}(x_k, c)) \tag{2}$$

where functions f and g respectively define the influence of *intra-region* energy and *inter-region* energy. The parameter $\alpha \in [0; 1]$ allows us to balance these two terms.

Figure 4 shows the influence of the two energies. If *intra-region energy* is decreased to the advantage of *inter-region energy*, split lines are mainly directed along highest gradient. Conversely, if *intra-region energy* is increased, split directions tend to be more homogeneously distributed. Indeed figure 4c displays a segmentation whose main split lines extract floors, whereas split lines of segmentation in figure 4a are less ordered.

3.2 *Intra-Region* Energy

We study now *intra-region* energy of vertical hypotheses. Horizontal hypotheses energy is computed in a similar way. *Intra-region* energy E_{intra} is based on the difference $\Delta(x_k, c_h)$ of

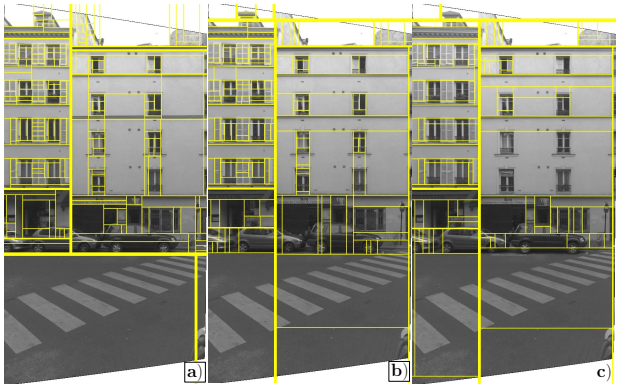

Figure 4: Influence of the α parameter on segmentation. a) $\alpha = 20\%$ b) $\alpha = 50\%$ c) $\alpha = 80\%$

regular edges density between both sides of the vertical line x_k (equation 3).

$$\Delta(x_k, c_h) = \sum_{j=1}^{m} \left(\frac{\sum_{i=1}^{k} c_h(i,j)}{x_k - x_0} - \frac{\sum_{i=k+1}^{n} c_h(i,j)}{x_n - x_{k+1}} \right)^2 \tag{3}$$

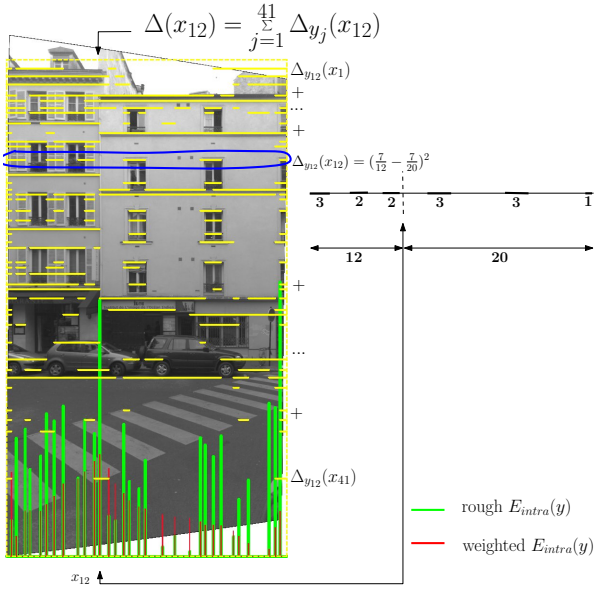

Figure 5: *Intra-region energy*. Yellow lines are horizontal regular edges. Bottom green profile illustrates rough *Intra-region energy* intensities, red one illustrates weighted *Intra-region energy* intensities. Split Hypothesis x_{12} is tested and one horizontal alignment (in cyan) is analyzed on the right of the image.

For instance figure 5 illustrates this computation on hypothesis x_{12}: one horizontal alignment is analyzed on the right of the image where left density is quite greater than right density. Bottom green profile displays all horizontal *regular edges* density differences. This measure unfortunately becomes unstable at region border. A peak occurs on right border because of small local *regular edges* on the right. We propose a compensation of this phenomenon displayed by red profile. We subtract the mean of density difference distribution. If all edges are supposed to have the same length, then the mean $\overline{\Delta}(x_k)$ of hypothesis x_k is $\sum_{c_h} p(c_h)\Delta(x_k, c_h)$. The result of this mean distribution is given by equation 4.

$$\overline{\Delta}(x_k) = p(1-p)\left(\frac{1}{x_k} + \frac{1}{n-x_k}\right) \quad (4)$$

with p being the probability of *regular edges* occurrence.

For practical purposes we fix the probability p to $\frac{1}{2}$: *regular edges* can appear everywhere in the region without any *a priori*. Figure 5 shows how this border compensation improves the process.

Figure 3b shows a vertical *intra-region* energy profile: the first extreme is located between the ground-floor and the first one, second extreme is located between the first floor and the second one. Split choice is then determined by *Inter-Region* Energy.

3.3 *Inter-Region* Energy

The *inter-region* energy evaluates the *regular edges* length along the split hypothesis under study. Equation 5 gives the *inter-region* of a vertical hypothesis x_k. Energy of horizontal hypotheses is computed in a similar way.

$$E_{inter}(x_k, c_v) = \sum_{j=1}^{m} c_v(i,j)\overline{v_{i,j}} \quad (5)$$

where $\overline{v_{i,j}}$ is the length of edge $v_{i,j}$.

This split energy term let process be directed by main gradient location. When some split hypotheses have analogous *intra-region energy*, *inter-region* energy is an accurate further selection criterion. For instance on figure 3b, this information is essential.

4 PERIODIC MODEL

Dominant alignments is a geometric property in common with most of facade architecture style. (Burochin et al., 2009) has verified that these alignments pretty rightly directs first steps of a hierarchical segmentation. But facades contains an other very frequent property that is actually missing in this previous approach: periodicity. We will see that accurate period hypotheses can be inferred from dominant alignments.

We introduce in this section a *periodic model* that is to considered as a *macro model*. Indeed it lets the process operate a kind of other models factorization. It assumes sub-image I_k to be composed of the periodic concatenation of a same sub-region that we name *kernel of the model*. A sub-figure composed of a window for instance could be the kernel of a model that represents a regular grid of similar windows (see figure 6).

General rules of our repetitive pattern detection resemble (Wenzel et al., 2008) but we do not look for any hierarchy in the periods. We only select the most frequent in horizontal and vertical directions: this restriction is sufficient because the process is recursive. We do not use the same interest points either: our points are intersections of dominant alignments.

An important aspect of the *periodic kernel* concept is the fact that this kernel is not an *irreducible region* as described in (Müller et al., 2007). This kernel is possibly composed by sub-patterns. This case occurs by instance in figure 6: kernel is composed of three similar windows. We first generate period hypotheses. Then we select the best one to try to build a *periodic kernel*.

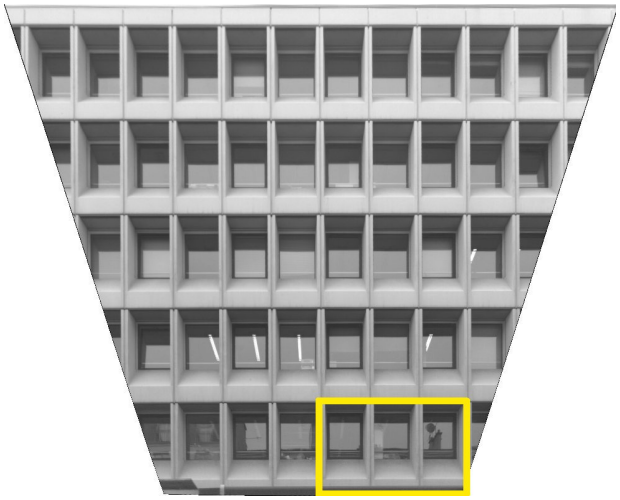

Figure 6: Periodic model of a window grid pattern with perspective effects and local occlusions: Three horizontally aligned windows framed in yellow constitute the kernel.

4.1 Period hypothesis Generation

Dominant alignments provide period hypotheses only with their coordinates whose distribution is partly regulated by main repetitive structures. We generate separately horizontal and vertical hypotheses. For vertical hypotheses, we accumulate all distances between horizontal dominant alignments to build a distance histogram. Figure 7 shows such a vertical distance histogram of region analyzed on figure 8. Horizontal distance histogram is computed in the same way.

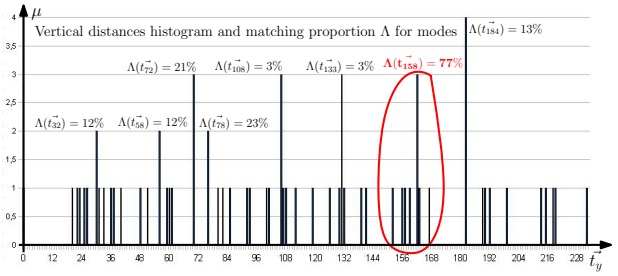

Figure 7: Distance histogram between horizontal dominant alignments of region displayed on figure 8. Each mode is related to the size of one repetitive pattern: matches proportions are mentioned. The best one is circled in red (floor size).

Each mode of these histograms is related to the fixed size of one repetitive pattern. Small distances concern small patterns (such as balconies, windows or gabs between two windows if the kernel is a floor). We are looking for the size of macro patterns that is the sum of those small patterns sizes. These macro-patterns are supposed to exactly partition the considered region.

4.2 Best Period selection

We have now to select one best period hypothesis. Solution that we have found is to correlate a significant number of key point pairs that satisfy three conditions:

1. homogeneous distribution in the region
2. stable locations
3. accurate matching measure

We build a set Π of key points from the intersection of dominant alignments (figure 8) that theoretically satisfy the two first conditions. Then we use *Pearson correlation* to match these points. Radiometric descriptors are enough to match similar points because points lay in one same rectified image. For an hypothesis $\vec{t_y}$ (respectively $\vec{t_x}$), we compute correlations between all pairs of points $(\Pi[i], \Pi[j])$ such that $\Pi[j] \simeq \Pi[i] + \vec{t_y}$ (respectively $\Pi[j] \simeq \Pi[i] + \vec{t_x}$). We select hypothesis $\vec{t_y^*}$ (respectively $\vec{t_x^*}$) whose matches proportion Λ^* is the best in the region. If $\Lambda^*(\vec{t})$ is high enough for the period $\vec{t_y^*}$ or the period $\vec{t_x^*}$, then the image I_k is considered as a periodic model whose kernel dimension is given by $(||\vec{t_x}||, ||\vec{t_y}||)$. If only one periodicity dimension X or Y is detected, then we respectively use the height or the width of the region to build the kernel. If no good matches proportion is detected, the region is assumed not matching any periodic model.

Figure 8 concerns a set of similar floors whose windows do not lay regularly in the region. Proportion $\Lambda(\vec{t_y^*})$ is high enough to consider the distance $||\vec{t_y^*}||$ - floor height - as a period whereas $||\vec{t_x^*}||$ is too low. Then the region is assumed to match a periodic model whose kernel is the floor.

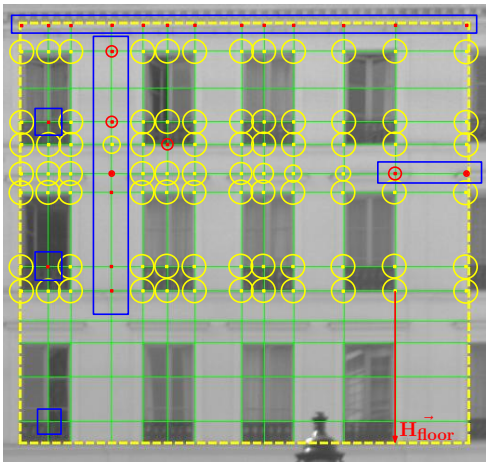

Figure 8: Matches of period $\vec{t_y^*} = \vec{H_{floor}}$. Dominant alignments are drawn in green. Correlation score $(\Pi[i] * \Pi[j])$ is illustrated by the length of the circle around $\Pi[i]$, where $\Pi[j] = \Pi[i] + \vec{t_y^*}$. A negative correlation score is illustrated as a point. Good correlation scores (greater than 80%) are circled in yellow; bad scores are circled in red. On 104 issues, 80 matches are correct. Blue rectangles are special cases.

This periodic model criterion is based on the essential hypothesis of a chaotic distribution of occlusions such as shutters, flowerpots or reflects, on the entire region. We do not delete such occlusion effects but we assume that proportion of hidden key points is insignificant compared with the total number of good matches. This restriction means that periodic model would be rejected when variations on repetitive patterns occur in the same location (homogeneous distributions of closed and open shutters, dense vegetation at foreground for example). But apart from such specific occurrences, periodicity is correctly detected. For instance in figure 8, a bad match occurs between a key point located on a closed window and a point on an opened window. Nevertheless good matches number is high enough to validate a periodic model.

Furthermore this correlation based criteria uses geometric and local radiometric clues. It is sufficient. We do not compute deviation $N_{\mathcal{M}_3}(I_k)$ between image I_k and a synthetic model M_3 in the same way than the planar and cylindric models given that periodic model takes into account a more global outlook of the facade. We voluntary ignore areas between key points in order to prevent perspective effects and local occlusions to disturb the matching process. Figure 6 shows a facade composed of windows in regular grid. The process matches its whole region as a periodic model despite perspective effects, strip lighting that sometimes appear behind window glass and reflects. Influence of these disruptions are naturally decreased by the reject of instable alignments. An alignment A is instable for a period $\vec{t}$ if there is no corresponding dominant alignments $A + \vec{t}$.

5 RESULTS AND DISCUSSION

On the same image, figure 9 shows hierarchical segmentation of (Burochin et al., 2009) compared to the new one. The former first separates the two facades whereas the latter separates facades from the ground level. Both choices are relevant but we notice that in a general way over-segmentations are prevented by the new split energy formulation and periodic models detection.

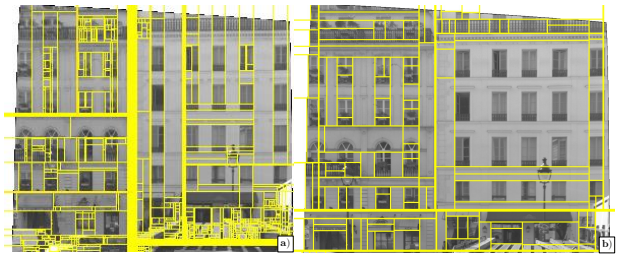

Figure 9: a) Hierarchical segmentation with dominant alignments detection in sub regions before split selection and without periodic model detection. b) Hierarchical segmentation proposed in this article.

This hierarchical segmentation still encounters some problems. The main one is that split process often breaks periodicity instead of framing it. On Figure 9b second, third and fourth floors of the right facade are identical. They are composed of five windows. On each floor, one single window lay on the left, three windows are centered and one single window lay on the right. The segmentation process do not frame the wall with all its content: it set apart single windows on the right from the rest of the identical floors. This phenomenon is due to split energy formulation that tend to break different contour densities.

A second problem of this approach is its dependence on rectifying process approximations that is directly reflected in *regular edges* detection and key points correlations. Objects are not exactly straight aligned. Twice condition on neighborhood stability of key point set obviously is not satisfied. For instance the two points $\Pi[i_1]$ and $\Pi[i_2]$ in blue rectangle on the right of figure 8 are not correctly matched with corresponding $(\Pi[i_1] + \vec{t_y^*})$ and $(\Pi[i_2] + \vec{t_y^*})$ because of rectifying imprecision.

Besides matches of key points located on uniform radiometries are hardly computed: blue vertical rectangle in figure 8 shows bad correlations because of too much noise. Third condition of key points set neither is verified. A consequence of this previous problems is that segmentation tends to separate floors before grouping them in a periodic model. Then most of estimated periods lay in only one dimension. Figure 10 shows a facade acquired from two different view points. First image is a crop of the big image displayed on figure 11. Second one is acquired from a closer view point such that only left part of the facade is shown. We notice high trend to separate floors in two cases. But floor internal segmentation hardly differs. For instance third and fourth floor are split into small parts on image 10a whereas they are grouped in a periodic models in image 10b. This phenomenon

can be explained by the difference of initial segmentation situation: considered floor width in image 10b is half as big than the one in whole image 11.

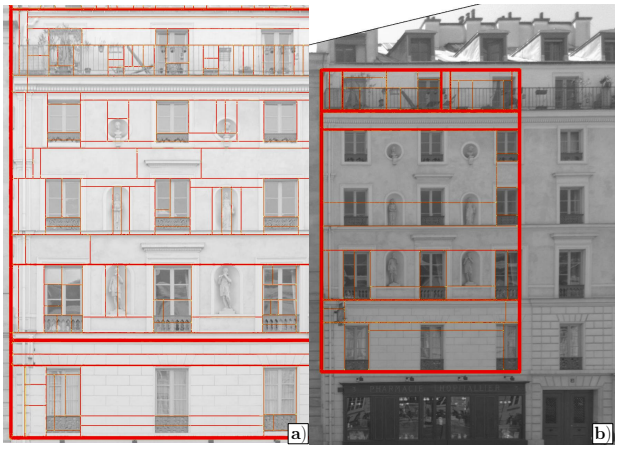

Figure 10: Hierarchical segmentation of a facade acquired from two different view points and cameras. a) Segmentation Crop of image displayed on figure 11. b) Segmentation of the same facade from a closer view point such that only left part is shown.

Moreover at small regions, key points number may be too small because of a fixed neighborhood length of dominant alignments. From all these limits we hold two main considerations. In the one hand split process is entirely independent of periodicity information. In the other hand periodicity estimation is based on correlation scores between points whose location does not depends on any local information.

6 CONCLUSIONS AND FUTURE WORK

In this paper, we have presented several improvements to the unsupervised model-based segmentation approach of (Burochin et al., 2009) that provide interesting results. It is able to separate a facade from its surroundings but also to organize the facade itself in a hierarchy. Dominant alignments are very fast to compute and provide good split hypotheses as well as good period hypotheses and an homogeneous distribution of key points. The detection of periodicity lets the process deal with local occlusions and perspective effects. Such an unsupervised segmentation will provide relevant clues to classify the facade architectural style or to detect objects behind or in front of it. It is also intended to give geometrical information that represents relevant indexation features *e.g.* windows gab lengths or floor delineation.

We have also introduced a model to detect periodicity that makes the segmentation more relevant. However, we also could add periodicity information in best split selection in order to prevent the process from breaking periodic structures before framing them. Besides we could put our key points on possibly local stable neighborhood such as corners with *Harris score* and reject uniform neighborhoods. Additionally we could subdivide the periodic kernel in *irreducible regions* in the same manner as (Müller et al., 2007). We then would detect local occlusions beforehand as residuals of a comparison between image information and information of the kernel. These *irreducible regions* could be matched by graph approach of (Haugeard et al., 2009) or we could compute a 3D polygonal model when considering perspective effects.

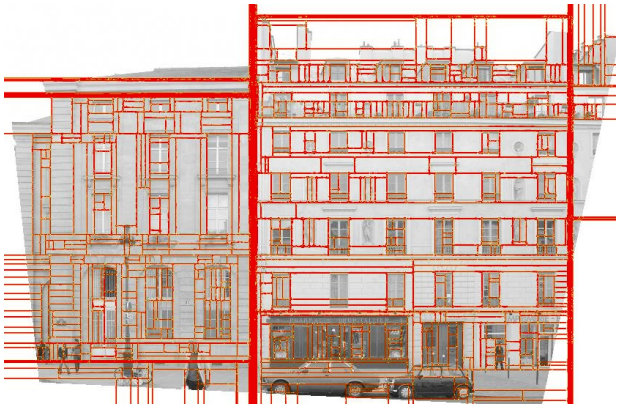

Figure 11: Hierarchical segmentation: split line thickness is proportional to segmentation depth.

REFERENCES

Alegre, F. and Dellaert, F., 2004. A Probabilistic Approach to the Semantic Interpretation of Building Facades. In: Proc. International Workshop on Vision Techniques Applied to the Rehabilitation of City Centres, Lisbon, Portugal. in electronic format only.

Ali, H., Seifert, C., Jindal, N., Paletta, L. and Paar, G., 2007. Window Detection in Facades. In: Proc. International Conference on Image Analysis and Processing, Vol. 14, International Association on Pattern Recognition, Modena, Italy, pp. 837–842.

Burochin, J.-P., Tournaire, O. and Paparoditis, N., 2009. An Unsupervised Hierarchical Segmentation of a Facade Building Image in Elementary 2D-Models. In: International Archives of Photogrammetry and Remote Sensing and Spatial Information Sciences, Vol. XXXVIII (Part 3/W4), Paris, France, pp. 221–228.

Han, F. and Zhu, S.-C., 2005. Bottom-up/top-down image parsing by attribute graph grammar. In: Proc. IEEE International Conference on Computer Vision, Vol. 10, Beijing, China, pp. 1778–1785.

Haugeard, J.-E., Philipp-Foliguet, S. and Precioso, F., 2009. Windows and facades retrieval using similarity on graph of contours. In: Proc. IEEE International Conference on Image Processing, Vol. 16, Cairo, Egypt. in electronic format only.

Kalantari, M., Jung, F., Paparoditis, N. and Guédon, J.-P., 2008. Robust and Automatic Vanishing Points Detection with their Uncertainties from a Single Uncalibrated Image, by Planes Extraction on the Unit Sphere. In: International Archives of Photogrammetry and Remote Sensing and Spatial Information Sciences, Vol. XXXVII (Part3A), Beijing, China, pp. 203–208 ff.

Korah, T. and Rasmussen, C., 2007. 2D Lattice Extraction from Structured Environments. In: Proc. International Confrence on Image Analyse and Recognition, Vol. 2, Montreal, Canada, pp. 61–64.

Lee, S. C. and Nevatia, R., 2004. Extraction and Integration of Window in a 3D Building Model from Ground View images. In: Proc. IEEE Conference on Computer Society Conference on Computer Vision and Pattern Recognition, Vol. 2, Minneapolis, Minnesota, USA, pp. 113–120.

Müller, P., Zeng, G., Wonka, P. and Gool, Luc, V., 2007. Image-based Procedural Modeling of Facades. ACM Transactions on Graphics 26(3), pp. 85.

Reznik, S. and Mayer, H., 2007. Implicit Shape Models, Model Selection, and Plane Sweeping for 3D Facade Interpretation. In: International Archives of Photogrammetry and Remote Sensing and Spatial Information Sciences, Vol. XXXVI (Part 3A), Munich, Germany, p. 173.

Ripperda, N., 2008. Determination of Facade Attributes for Facade Reconstruction. In: International Archives of Photogrammetry and Remote Sensing and Spatial Information Sciences, Vol. XXXVII (Part3A), Beijing, China, pp. 285–290.

Wenzel, S., Drauschke, M. and Frstner, W., 2008. Detection of repeated structures in facade images. Pattern Recognition and Image Analysis 18(3), pp. 406–411.